A Low-Profile Wideband LTCC Integrated Circularly Polarized Helical Antenna Array for Millimeter-Wave Applications

Ming DU [1], Jun XU [1], Xiao DING [1], Jiangping CAO [2], Jianhua DENG [2], Yuliang DONG [2]

[1] School of Physical Electronics, University of Electronic Science and Technology of China, Chengdu, China
[2] National Institute of Measurement and Testing Technology of China, Chengdu, China

mingdu_uestc@163.com, xujun@uestc.edu.cn, xding@uestc.edu.cn, jh_deng@126.com, 1878281644@qq.com, dongyull@163.com

Submitted June 4, 2017 / Accepted January 15, 2018

Abstract. *A low-profile wideband low-temperature co-fired ceramic integrated circularly polarized helical antenna array for millimeter-wave applications is presented. The major consideration of the antenna element design is to achieve good circular polarization and wide bandwidth when the helix has just about one turn which is beneficial for low profile. The turn is composed of 6 × 1/5-turn horizontal segments with straight-edge connections implemented by via holes. A 2 × 2 helical antenna array with a dimension of 25 × 15 × 1.316 (0.15λ_0, is the wavelength at 35 GHz) mm^3 is also designed. The simulated results show that the proposed helical antenna array has a wide impedance bandwidth from 26.5 to 40 GHz for $|S_{11}| < -13$ dB and AR < 3 dB. The proposed antenna array was also measured and good agreement is achieved between the simulated and measured results.*

Keywords

Millimeter-wave (mmW), circularly polarized, helical, array, low-temperature co-fired ceramic (LTCC)

1. Introduction

Recently, circularly polarized (CP) antennas are receiving more and more attention in millimeter-wave (mmW) applications because of the suppression of the multipath reflection, reduction of the polarization mismatch, etc. [1], [2]. Besides, the electromagnetic signal can be always received by CP antennas no matter the transmitting antenna is rotating or not. Various CP antennas have been reported over past decades such as CP patch antennas [3], [4], helical antennas [5], CP horn antennas [6], CP wide slot antennas [7], spiral antennas [8], crossed dipole antennas [9], and so on. Among them, helical antennas can exhibit good circular polarization, excellent directivity, high gain and wide bandwidth, which are required in many mmW applications. However, traditional helical antennas have extremely high profile.

Planar helical antennas can overcome the shortcoming easily. A planar helical antenna with low profile (0.11 wavelength at 10 GHz), wide impedance and axial ratio (AR) bandwidth operating at 10 GHz was investigated in [10]. The helix was formed using printed strips with straight-edge connections implemented by via holes, and a planar cavity was also designed to improve the radiation pattern. Nevertheless, the radiation pattern is end-fire, so the antenna is difficult to be applied to two-dimensional (2-D) arrays in a single substrate for some applications such as the 2-D planar phased scanning. A low-profile and wideband helical antenna is proposed in [11], but its structure is complex and it is not suitable for integration. [12] presents a small-size, low-profile, and low-cost helical antenna. However it works in normal mode, therefore it cannot radiate circularly polarized wave. It should be noted that in [13] and [14], two low-temperature co-fired ceramic (LTCC) helical antenna arrays working at 60 and 94 GHz respectively with broadside radiation pattern and good circular polarization performance were reported. As a multilayer technology, the LTCC technology is a good choice for mmW applications owing to its advantages of light weight, compactness, convenient integration, easy realization of the blind vias which makes the helix to be fabricated easily, excellent high frequency performance and high temperature resistance. Whereas, in order to achieve good circular polarization performance, more turns were used in these two helical antennas, thus the profile is still high (0.38 wavelength at 60 GHz in [13], 0.62 wavelength at 94 GHz [14]).

In this work, the main challenge and novelty are reducing the number of the LTCC layers while keeping good circular polarization. In order to achieve this goal, a one-turn helical antenna with broadside radiation on LTCC is proposed as an element of a helical antenna array working at Ka-band. Instead of increasing the number of helical turns to obtain good circular polarization, more segments were constructed in one helical turn while maintaining the number of the helical turn being just one. The total thickness of the proposed antenna is just 0.15 λ_0 (λ_0 is the wavelength at 35 GHz). Then, a 2 × 2 helical array was fabricated and measured.

2. Antenna Element Design

2.1 Configuration and Performances

The 3D, top and side views of the proposed antenna element are shown in Fig. 1. The multilayer LTCC substrate used is Ferro A6-M with dielectric permittivity $\varepsilon_r = 5.9 \pm 0.2$ and loss tangent $\tan\delta = 0.002$ at 35 GHz. Each LTCC layer has a thickness of 0.094 mm. The conductor thickness is 0.01 mm. The proposed helical antenna has just about one-turn helix which is composed of $6 \times 1/5$-turn horizontal segments lying on different layers of the LTCC substrate. The horizontal segment is ring-shaped and the neighboring horizontal segments were connected by via holes with each other. The lowest horizontal segment is connected to the microstrip by a via hole through a circular aperture on the ground. The antenna is fed by the microstrip. In order to reduce the total number of layers and integrate active components easily, the feeding microstrip is single-layer. The width of the feeding microstrip line w_1 was chosen to be 0.15 mm, which corresponds to the characteristic impedance of 50 Ω, and the diameter of all via holes is 0.1 mm. The detailed dimensions are shown in Tab. 1.

The AR of a traditional helical antenna working in axial mode can be expressed as [15]:

$$AR = \frac{2N+1}{2N} \tag{1}$$

where N is the number of the turns.

To achieve good circular polarization, the circumference of the helix must be in the range of $3/4 < C/\lambda_g < 4/3$, where C is the perimeter of the turn, and λ_g is the wavelength in the substrate mixed of air and LTCC, so ε_{mr} of the mixed substrate should be in the range of 1 to 5.9 and λ_g should be in the range of 3.53 to 8.57 mm at 35 GHz. Moreover, the relationship between h and w_2 shown in Fig. 1 can be expressed as [16]:

$$h = \frac{w_2}{\left(\dfrac{377}{\sqrt{\varepsilon_{mr}}\sqrt{\varepsilon_r}Z_0}\right) - 2} \tag{2}$$

where Z_0 is the characteristic impedance of the feeding microstrip line. Therefore, when w_2 and Z_0 are determined, then h can be calculated. According to the dimensions shown in Tab. 1, the results of the formulas above can be computed as:

$$\frac{2N+1}{2N} = \frac{2\times\frac{6}{5}+1}{2\times\frac{6}{5}} \approx 1.416,$$

$$AR = \left|10\log_{10}(1.416)\right| = 1.5 \text{ dB},$$

$$h = \frac{0.2 \text{ mm}}{\left(\dfrac{377}{\sqrt{\varepsilon_{mr}}\sqrt{5.9}\times 50}\right) - 2} \approx (0.2 \sim 0.49) \text{ mm}.$$

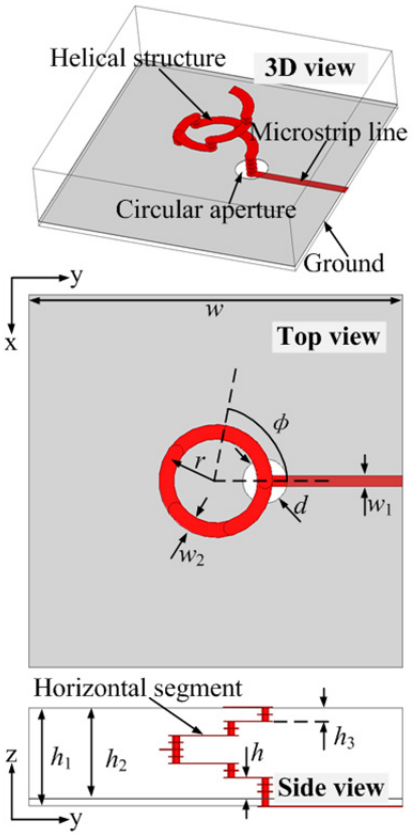

Fig. 1. 3D, top and side views of the proposed antenna element (antenna 3).

Parameter	Value	Unit
w	5	mm
d	0.6	mm
Φ	72	degree
w_1	0.15	mm
w_2	0.2	mm
r	0.66	mm
h (3 layers)	0.282	mm
h_1 (13 layers)	1.316	mm
h_2 (14 layers)	1.222	mm
h_3 (2 layers)	0.188	mm

Tab. 1. Detailed proposed antenna element dimensions.

It should be noted that all of the above results are based on a rough computation because of the significant difference between the traditional helical antenna and the helical antenna fabricated using LTCC technology.

The simulated $|S_{11}|$, AR and gain of the proposed antenna element are depicted in Fig. 2. It can be seen that, from 25 to 40 GHz, the $|S_{11}|$ is less than –15.1 dB. The 3-dB AR bandwidth is 49.6% from 25.8 to 42.8 GHz covering all the Ka-band. And the gain is about 5 dBi with slight fluctuations over the frequency range of 25 to 40 GHz.

The radiation patterns at 27, 35 and 40 GHz of the proposed antenna element are plotted in Fig. 3. As the helix is right-handed, the right-hand circularly polarized (RHCP) wave is generated as the co-polarization in both planes while the left-hand circularly polarized (LHCP) wave is generated as the cross-polarization. The front-to-back ratios (FBRs) are 22.2, 20.3 and 23.1 dB at 27, 35 and 40 GHz.

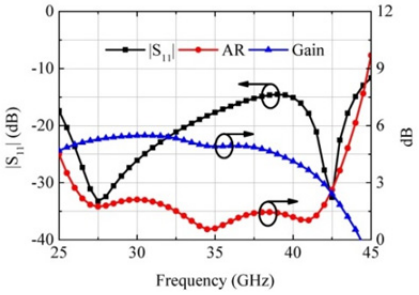

Fig. 2. Simulated $|S_{11}|$, AR and gain of the proposed antenna element.

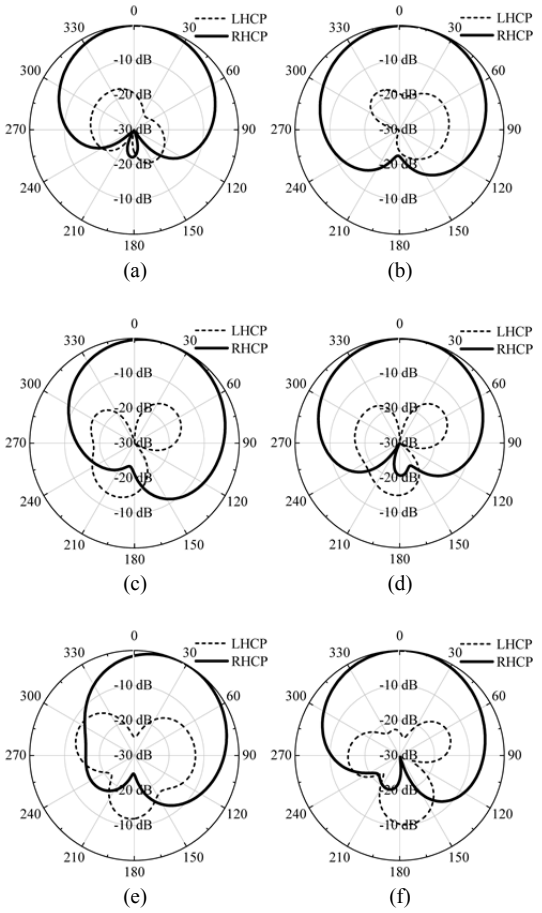

Fig. 3. Radiation patterns of the proposed antenna element at (a) XOZ-plane at 27 GHz; (b) YOZ-plane at 27 GHz; (c) XOZ-plane at 35 GHz; (d) YOZ-plane at 35 GHz; (e) XOZ-plane at 40 GHz; (f) YOZ-plane at 40 GHz.

The FBR is high even the helical antenna is fed by microstrip line.

2.2 Evolution and Working Principle

The evolution of the proposed antenna element is shown in Fig. 4. All the parameters of these helical antennas are the same except the total number of layers (almost the same), the number of the horizontal segments N and the degree Φ (in fact, there is a one to one correspondence between N and Φ), therefore they work in the same frequency range. The comparisons of the simulated $|S_{11}|$s and ARs of the four helical antennas are depicted in Figs. 5 and 6. It can be seen that, with the increasing of N, the geometry of the multilayered helical antenna becomes more and more close to a traditional one. However, the optimal result is not obtained when N equals to the maximum limit value (one segment occupies single layer).

To illustrate this phenomenon, the top views of the current distributions on the helixes of antennas 3 and 4 at different frequencies are plotted in Fig. 7. As shown, the number of the helical turn of antenna 3 occupied by the half-period current changes less in the frequency range of 26 to 42 GHz than that of antenna 4, which indicates that the current mode on antenna 3 is more stable. As a result, the performances of antenna 3 are more stable and the antenna 3 is easier to achieve wider impedance and AR bandwidths. Besides, compared with antennas 3 and 4, the deviation of antennas 1 and 2 from a traditional helical antenna is too much and the current modes on them are either not stable, so the performances of antennas 1 and 2 are worse than that of antenna 3 either. The current distributions on the helixes of antennas 1 and 2 are not shown here for brevity. So antenna 3 achieves the best performance.

In fact, the via holes for straight-edge connections between adjacent horizontal segments will introduce parasitic capacitances and inductances. The values of these parasitic capacitances and inductances depend on the dimensions of these via holes and the heights of the via holes, which are determined by N. These parasitic capacitances and inductances will introduce extra phase delay. Therefore different N means different phase delays. And only proper N can compensate the change of the helical turn occupied by the half-period current caused by frequency variation.

Table 2 displays the phase delay between the beginning and completion of the current reversal on these via holes, which also can be defined as the phase delay of the current node getting through the via hole or the phase delay of the current caused by these via holes. From Tab. 2, the phase delay of the current caused by the via hole of antenna 3 changes little in the frequency range of 26 to 42 GHz, which can compensate the change of the helical turn occupied by the half-period current caused by frequency variation. As a result, the current mode on antenna 3 is stable. On the other hand, the phase delay of the current caused by the via hole of antenna 4 changes great and the number of the via holes of antenna 4 is more than that of antenna 3, thus the current mode on antenna 4 is not stable.

The steps of the antenna design are shown below:

1. according to the conditions to achieve good circular polarization described in Sec. 2.1, select the circumference of the helix.
2. according to (2), design the feeding structure to match the 50-Ω feeding microstrip.
3. make sure the number of the helix turn is near 1 for low profile and built the possible antenna structure with different number of horizontal segments.
4. simulate the whole antenna and tune slightly for the best circular polarization performance.

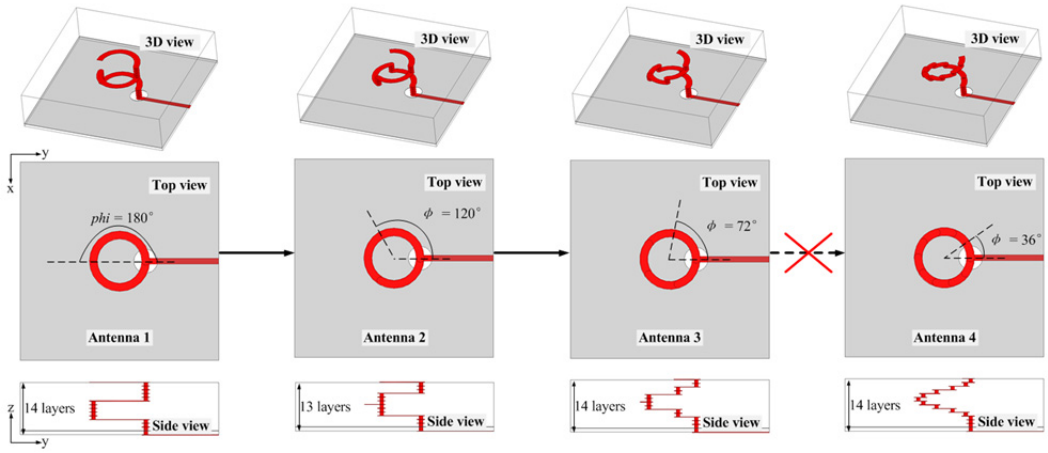

Fig. 4. Evolution of the proposed antenna element.

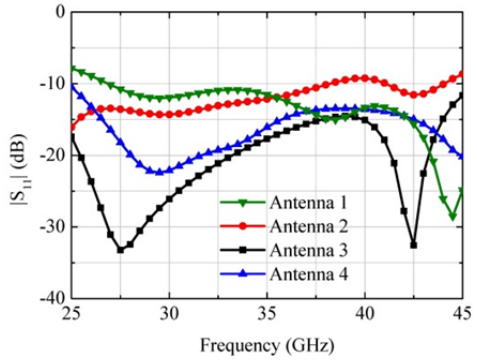

Fig. 5. Comparisons of the simulated $|S_{11}|$s of the four helical antennas.

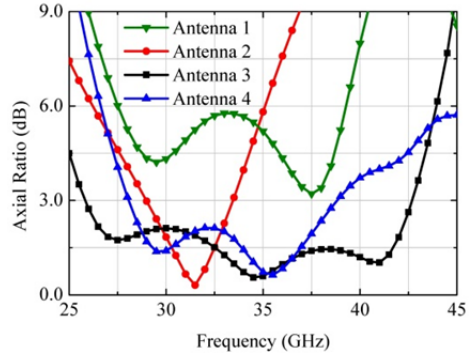

Fig. 6. Comparisons of the simulated ARs of the four helical antennas.

Helical antenna	26 GHz	35 GHz	42 GHz
Antenna 3	30°	30°	35°
Antenna 4	13°	24°	47°

Tab. 2. Phase delay by the via holes for straight-edge connections between adjacent horizontal segments.

2.3 Parameter Study

Effects of the *h, r* and w_2 of antenna 3 on $|S_{11}|$ and AR are studied, as shown in Fig. 8. From Fig. 8, the 3-dB AR band is shifted to higher frequencies with the increasing of the height *h*, and the best performance is obtained when $h = 0.282$ mm. When the radius *r* of the helix increases, the

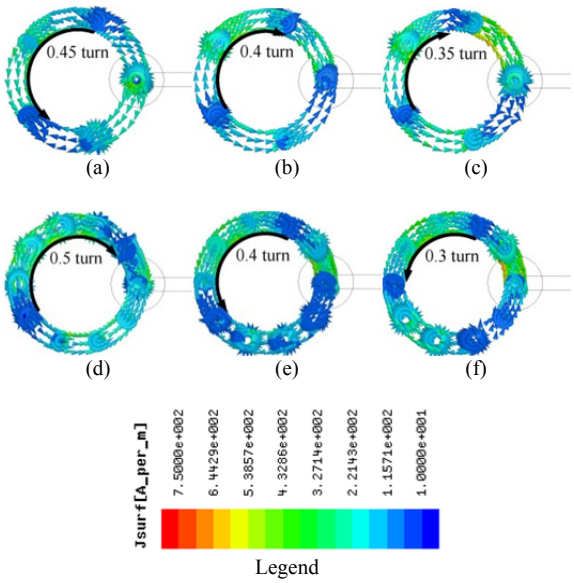

Fig. 7. Top views of the current distributions on the helixes of antenna 3 at (a) 26 GHz, (b) 35 GHz, (c) 42 GHz, and antenna 4 at (d) 26 GHz. (e) 35 GHz. (f) 42 GHz.

bandwidths of both $|S_{11}|$ and AR shift to lower frequencies and the AR of lower frequencies deteriorates quickly. The bandwidths of both $|S_{11}|$ and AR are widened as the width w_2 of helix increases, and the best performance is achieved when w_2 is equal to 0.2 mm.

3. Antenna Array Design

Figure 9(a) shows the geometry of the proposed antenna array. For increasing the adhesion between adjacent layers of LTCC, the grounds located on the edge of the antenna array which have little effect on the performance of the antenna array were removed. A planar parallel microstrip line feeding network was used to feed the 2×2 antenna elements with equal amplitude and phase. The size of the antenna array is 15×25 mm^2, and the thickness is 1.316 mm. The inner-element spacing of the antenna array is 4.1 mm ($0.48\lambda_0$).

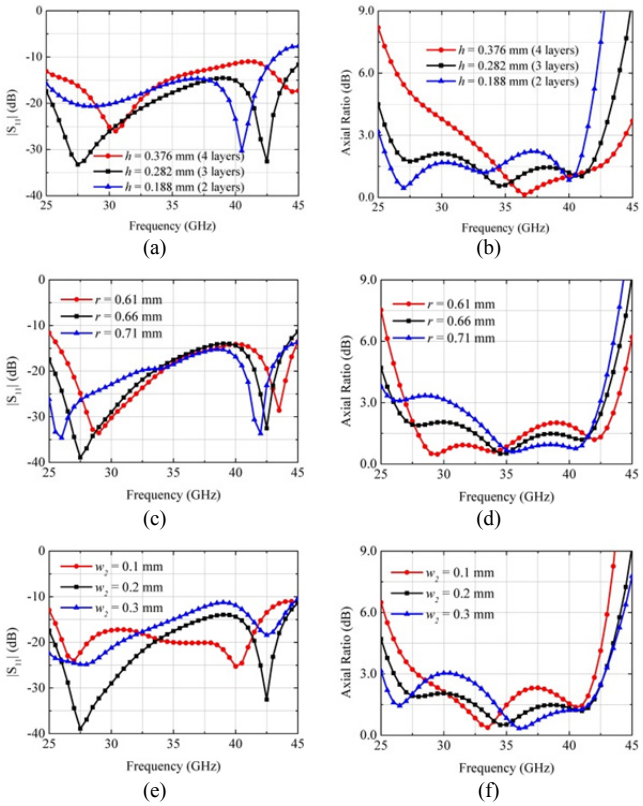

Fig. 8. Effects of the dimensions of antenna 3 on $|S_{11}|$ and AR, (a) h on $|S_{11}|$, (b) h on AR, (c) r on $|S_{11}|$, (d) r on AR, (e) w_2 on $|S_{11}|$, (f) w_2 on AR.

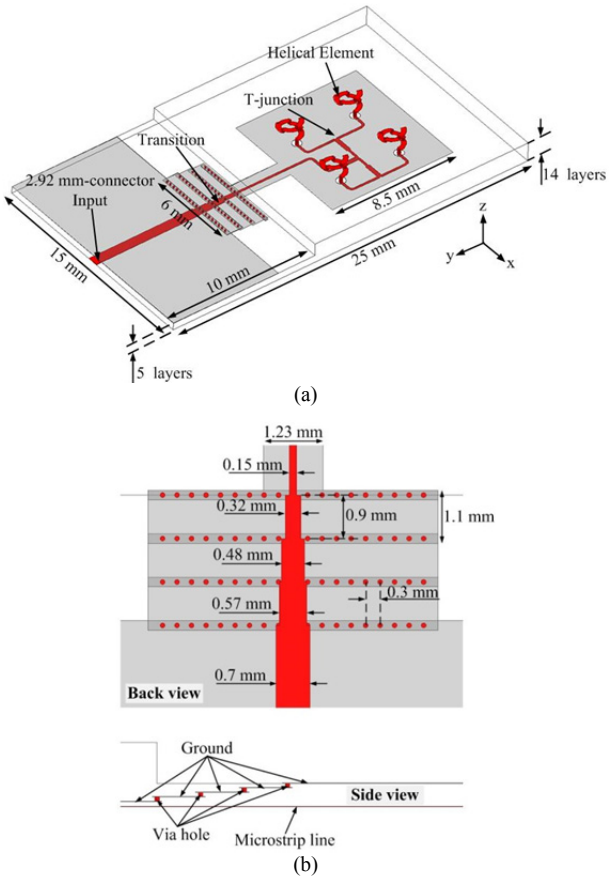

Fig. 9. (a) Geometry of the proposed 2 × 2 helical antenna array; (b) back and side views of the transition.

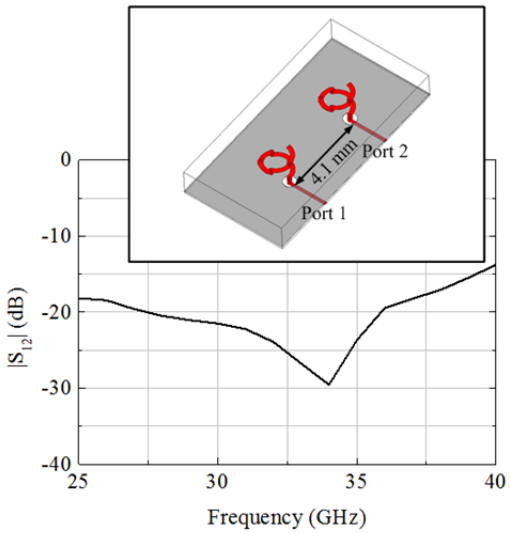

Fig. 10. Simulated $|S_{12}|$ of a 1 × 2 array.

A 2.92-mm connector was used to measure the performance of the antenna, and in order to weld the 2.92-mm connector easily, a transition between microstrips with different thicknesses, as shown in Fig. 9(b), was designed to widen the width of the microstrip. The detailed design principle, process and simulated results had been illustrated in our paper [17], so they are not illustrated here for brevity.

For illustration of the mutual coupling, the simulated $|S_{12}|$ of a 1 × 2 array is shown in Fig. 10. As observed, the simulated $|S_{12}|$ is less than –15 dB from 25 to 40 GHz, indicating the mutual coupling is relatively low.

4. Measured Results and Discussions

To verify the simulations above, an antenna array prototype was built and measured. Photographs of the antenna array prototype are given in Fig. 11(a), and the measurement equipment is shown in Figs. 11(b) and (c). Noted that only the $|S_{11}|$ below 40 GHz, AR and gain in the range of 27 to 39 GHz were measured because of the limitation of the experimental equipment. The simulated and measured $|S_{11}|$s, ARs and gains are shown in Fig. 12. It can be seen that the measured and simulated $|S_{11}|$s agree with each other reasonably. The measured $|S_{11}|$ of the proposed antenna array is lower than –13 dB from 26.5 to 40 GHz as shown in Fig. 12(a). Meanwhile, the measured AR from 27 to 39 GHz is lower than 4 dB as shown in Fig. 12(b), the simulated and measured results agree with each other relatively well. In addition, the antenna array achieves a peak gain 9.5 dBi at 37 GHz with a fluctuation of 3 dB over 31 to 39 GHz frequency range as shown in Fig. 12(c). The discrepancy between the simulated and measured gain is mainly caused by the loss of the transition from the feeding microstrip line to 2.92-mm connector and the differences of the radiation patterns between the simulated and measured results. The loss of the 2.92-mm connector is about 1.5 dB as demonstrated in our paper [18] and the simulated and measured radiation patterns at 27, 35, and 39 GHz are indicated in Fig. 13.

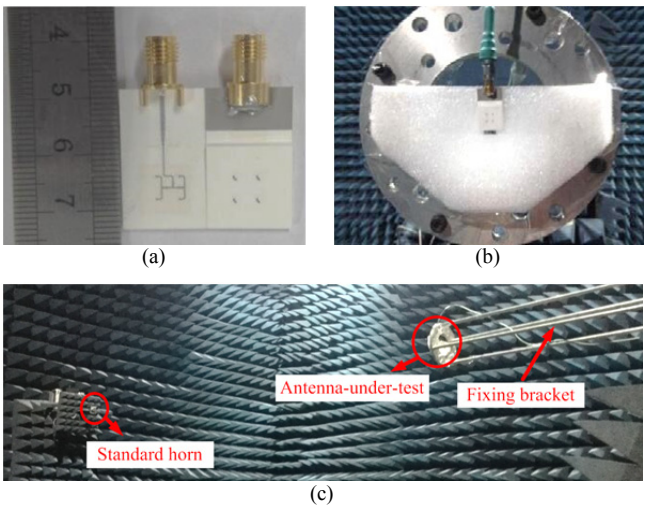

Fig. 11. (a) Photographs of the antenna array; (b) photographs of the measurement equipment (near view); (c) photographs of the measurement equipment (far view).

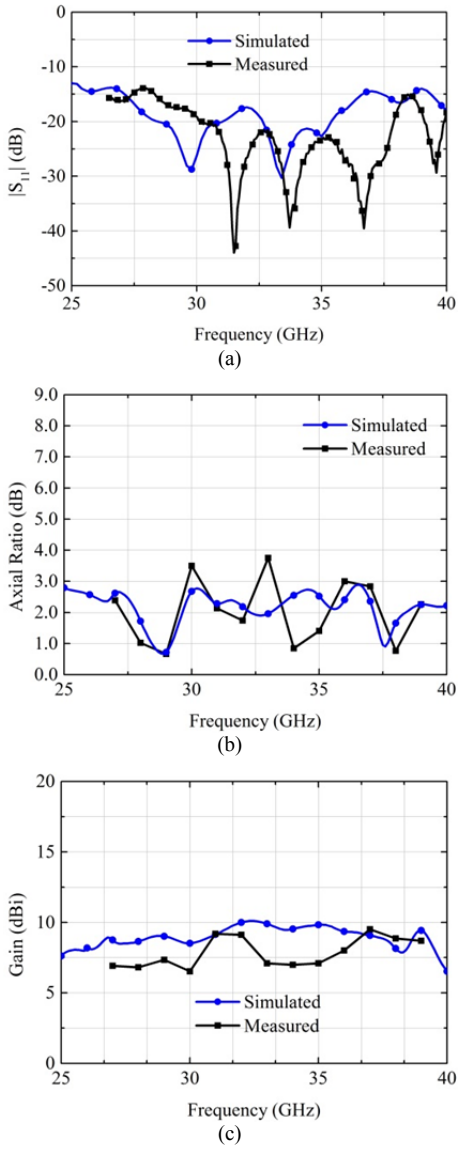

Fig. 12. Simulated and measured (a) $|S_{11}|$s, (b) ARs and (c) gains of the proposed antenna array.

As shown in Fig. 12(c), the differences of the gains are minimal at 31 and 37 GHz whereas at 34 GHz the difference is about 2.5 dB. This is because the measured beam widths are narrower than the simulated ones at low and high frequencies as shown in Fig. 13(a), (b), (e) and (f), and this can increase the gain. Therefore, the differences are minimal at 31 and 37 GHz. At middle frequency, the measured beam widths are slightly wider than the simulated one as shown in Fig. 13(c) and (d), and this can decrease the gain. Therefore, at 34 GHz the difference is big.

Only the radiation patterns in the upper-half plane are given because of the limitation of the measurement equipment. And it can be seen that when the angle approaches to 0°, the measured and simulated radiation patterns agree with each other well. However, when the angle approaches to 90° and –90°, they do not agree with each other so well. This may be attributed to the metal bracket for fixing the antenna array as shown in Fig. 11(b). The metal bracket is too close to the antenna array. The other differences between the measured and simulated radiation patterns may be caused by the fabrication and measurement error.

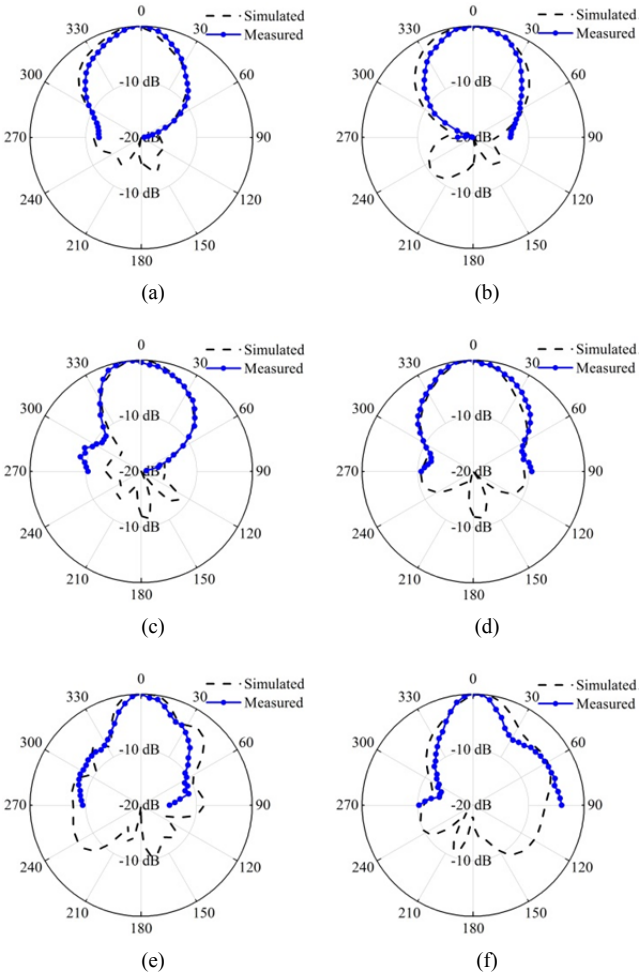

Fig. 13. Simulated and measured radiation patterns of the antenna array, (a) XOZ-plane at 27 GHz, (b) YOZ-plane at 27 GHz, (c) XOZ-plane at 35 GHz, (d) YOZ-plane at 35 GHz, (e) XOZ-plane at 39 GHz, (f) YOZ-plane at 39 GHz.

Helical arrays	Array in [13]	Array in [14]	This work
Center frequency	60 GHz	94 GHz	35 GHz
No. of elements	4 × 4	2 × 2	2 × 2
Total No. of layers	20 (0.38 λ_0)	21 (0.62 λ_0)	14 (0.15 λ_0)
No. of layers of radiator	15 (0.29 λ_0)	16 (0.47 λ_0)	13 (0.14 λ_0)
AR BW sim/mea	23.7%/20%	22.2%/-	46.2%/(over 36.4% for AR ≤ 4 dB)
Maximum measured gain	15 dBi	-	9 dBi

Tab. 3. Performance comparison of reported LTCC helical antenna arrays.

Table 3 lists the data of the antenna array proposed in this paper and other reported helical antenna arrays using LTCC technology. A comparison between two helical antenna arrays working at 60 and 94 GHz respectively and helical antenna array proposed was made because all the antenna arrays were fabricated using the same type LTCC. It can be seen that the antenna array proposed in this paper works at the lowest frequency band, it can achieve the least layers and the widest simulated 3-dB AR bandwidth.

5. Conclusion

In this paper, a LTCC circularly polarized helical antenna is proposed with wide impedance and AR bandwidth covering all the Ka-band. Then, a 2 × 2 antenna array was fabricated and measured. Compared with other work, the proposed antenna array has less layers and wider impedance and AR bandwidth. The proposed antenna array can be used in mmW applications.

Acknowledgments

This work was supported by the National Natural Science Foundation of China (No. 61401065), and the China Scholarship Council (CSC).

References

[1] JOHNSON, D. R., VOLAKIS, L. *Antenna Engineering Handbook*. 4nd ed. New York (USA): McGraw-Hill, 2007, p. (26-1)–(26-10). ISBN: 978-0071475747

[2] MANABE, T., SATO, K., MASUZAWA, H., et al. Polarization dependence of multipath propagation and high-speed transmission characteristics of indoor millimeter-wave channel at 60 GHz. *IEEE Transactions on Vehicular Technology*, 1995, vol. 44, no. 2, p. 268–274. DOI: 10.1109/25.385918

[3] HUANG, J. Microstrip antenna developments at JPL. *IEEE Antennas and Propagation Magazine*, 1991, vol. 33, no. 3, p. 33–41. DOI: 10.1109/74.88219

[4] PAN, Y. M., ZHENG, S. Y., HU, B. J. Wideband and low-profile omnidirectional circularly polarized patch antenna. *IEEE Transactions on Antennas and Propagation*, 2014, vol. 62, no. 8, p. 4347–4351. DOI: 10.1109/TAP.2014.2323412

[5] WHEELER, H. A. A helical antenna for circular polarization. *Proceedings of the IRE*, 1947, vol. 35, no. 12, p. 1484–1488. DOI: 10.1109/JRPROC.1947.234573

[6] MA, X., HUANG, CH., PAN, W., et al. A dual circularly polarized horn antenna in Ku-band based on chiral metamaterial. *IEEE Transactions on Antennas and Propagation*, 2014, vol. 62, no. 4, p. 2307–2311. DOI: 10.1109/TAP.2014.2301841

[7] ROW, J. S., WU, S. W. Circularly-polarized wide slot antenna loaded with a parasitic patch. *IEEE Transactions on Antennas and Propagation*, 2008, vol. 56, no. 9, p. 2826–2832. DOI: 10.1109/TAP.2008.928769

[8] NAKANO, H., OYANAGI, H., YAMAUCHI, J. A wideband circularly polarized conical beam from a two-arm spiral antenna excited in phase. *IEEE Transactions on Antennas and Propagation*, 2011, vol. 59, no. 10, p. 3518–3525. DOI: 10.1109/TAP.2011.2163759

[9] BAIK, J. W., LEE, K. J., YOON, W. S., et al. Circularly polarised printed crossed dipole antennas with broadband axial ratio. *Electronics Letters*, 2008, vol. 44, no. 13, p. 785–786. DOI: 10.1049/el:20080794

[10] CHEN, Z., SHEN, Z. Planar helical antenna of circular polarization. *IEEE Transactions on Antennas and Propagation*, 2015, vol. 63, no. 10, p. 4315–4323. DOI: 10.1109/TAP.2015.2463746

[11] QU, X, YANG, Z. The design of helix antenna on low profile and wide band. In *2016 IEEE 5th Asia-Pacific Conference on Antennas and Propagation (APCAP)*. Kaohsiung (Taiwan), 2017, p. 123–124. DOI: 10.1109/APCAP.2016.7843129

[12] LOPEZ-SORIANO, S, PARRON, J. Design of a small-size, low-profile and low-cost normal mode helical antenna for UHF RFID wristbands. *IEEE Antennas and Wireless Propagation Letters*, 2017, vol. 16, p. 2074–2077. DOI: 10.1109/LAWP.2017.2696300

[13] LIU, C., GUO, Y. X., BAO, X., XIAO, S. Q. 60-GHz LTCC integrated circularly polarized helical antenna array. *IEEE Transactions on Antennas and Propagation*, 2012, vol. 60, no. 3, p. 1329–1335. DOI: 10.1109/TAP.2011.2180351

[14] CAO, B., WANG, H., WANG, Y., ZHENG, J., et al. W-band LTCC helical antenna array with substrate integrated horn. In *2014 Asia-Pacific Microwave Conference*. Sendai (Japan), 2014, p. 357–359.

[15] BALANIS, C. A. *Antenna Theory*. 3nd ed. Hoboken (NJ): Wiley, 2005. P. 568–571. ISBN: 978-0471667827

[16] KRAUS, D. J., MARHEFKA, R. J. *Antennas: For All Applications*. 3rd ed. New York (NY, USA): McGraw-Hill, 2002. ISBN: 978-0072321036

[17] DU M., XU J., DONG Y. L., DING X. LTCC SIW-vertical-fed-dipole array fed by microstrip network with tapered microstrip-to-SIW transition for wideband millimeter-wave applications. *IEEE Antennas and Wireless Propagation Letters*, 2017, vol. 16, p. 1953–1956. DOI: 10.1109/LAWP.2017.2690325

[18] DU, M., DONG, Y. L., XU, J., DING, X. 35-GHz wideband circularly polarized patch array on LTCC. *IEEE Transactions on Antennas and Propagation*, 2017, vol. 65, no. 6, p. 3235–3240. DOI: 10.1109/TAP.2017.2689073

About the Authors ...

Ming DU was born in China in 1989. He received the B.S. degree in Electrical Engineering from the University of Electronic Science and Technology of China (UESTC) Chengdu, China, in 2011, and is currently pursuing the Ph.D. degree in UESTC. His research interests include microwave wave circuits and antennas.

Jun XU was born in China in 1963. He received the B.S. degree in 1984, and M.S. degree in 1990 from the University of Electronic Science and Technology of China (UESTC), Chengdu, China. He engaged in basic research in the field of radio physics subject and teaching work. He was hired as an associate professor in 1997, then as a professor in 2000 in UESTC. His main research interests include microwave theory and technology, millimeter-wave hybrid integrated technology, millimeter-wave communication and radar radio frequency technology. He has published over 80 papers in refereed journals.

Xiao DING was born in Sichuan, China, in 1982. He received the Ph.D. degree in Radio Physics from the University of Electronic Science and Technology of China (UESTC), Chengdu, China, in 2013. He joined UESTC in 2014, where he is currently an associate professor. He has been a Visiting Scholar at the South Dakota School of Mines and Technology, USA, a Visiting Fellow with the University of Houston, USA. His research interests include wide-angle scanning phased array, LTCC millimeter wave array and reconfigurable antenna and its applications.

Jiangping CAO was born in Xinjiang, China, in 1981. She received the bachelor's degree in Mechanical Design, Manufacturing and Automation, from the School of Mechanical Engineering of the East China Jiaotong University, Nanchang, in 2004, and master's degree in Software Engineering from the University of Electronic Science and Technology of China in 2014. She is currently an engineer with the National Institute of Measurement and Testing Technology, China. Her research interests include the design and development of automation, electromechanical integration and intelligent equipment.

Jianhua DENG was born in Jiangxi, China, in 1977. He received the M.Sc. and Ph.D. degrees in Radio Physics from the University of Electronic Science and Technology of China (UESTC), Chengdu, China, in 2003 and 2007, respectively. From 2001 to 2006, he was a research assistant with the Millimeter-wave Laboratory, Southwest Institute of Electronic Technology of China, Chengdu, China. In 2009, he was an associate professor with the School of Physical Electronics, UESTC, and a research fellow with the Department of Electronic Engineering, City University of Hong Kong, Kowloon, Hong Kong. From 2010 to 2011, he was a post doctor with the Department of Electronic and Computer Engineering, Duke University, Durham, NC, USA. He is currently an associate professor with the National Institute of Measurement and Testing Technology, China. His current research interests are in the areas of optimization, modeling, and computer-aided design for microwave and millimeter-wave integrated circuits and antennas.

Yuliang DONG was born in Sichuan, China, in 1972. He received the B.S. degree in Electronic Engineering from the Northwestern Polytechnical University, Xi'an, China, in 1993, and Ph.D. degree from Beihang University, Beijing, in 2005. He is currently an associate professor with the National Institute of Measurement and Testing Technology, China. His research interests include microwave wave circuits, passive components, antennas and microwave CAD technology.